NANO LETTERS

Letter

Cite This: Nano Lett. 2019, 19, 7703−7711

pubs.acs.org/NanoLett

# Spherical Nanovesicles Transform into a Multitude of Nonspherical Shapes

Rikhia Ghosh,[†] Vahid Satarifard,[†] Andrea Grafmüller, and Reinhard Lipowsky*

Theory & Biosystems, Max Planck Institute of Colloids and Interfaces, 14424 Potsdam, Germany

Supporting Information

**ABSTRACT:** Nanovesicles are closed, bubblelike surfaces with a diameter between 20 and 200 nm, formed by lipid bilayers and biomembranes. Electron microscopy (EM) studies have shown that these vesicles can attain both spherical and nonspherical shapes. One disadvantage of EM methods is that they provide only a single snapshot of each vesicle. Here, we use molecular dynamics simulations to monitor the morphological transformations of individual nanovesicles. We start with the assembly of spherical vesicles that enclose a certain volume of water and contain a certain total number of lipids. When we reduce their volume, the spherical vesicles are observed to transform into a multitude of nonspherical shapes such as oblates and stomatocytes as well as prolates and dumbbells. This surprising polymorphism can be controlled by redistributing a small fraction of lipids between the inner and outer leaflets of the bilayer membranes. As a consequence, the inner and the outer leaflets experience different mechanical tensions. Small changes in the vesicle volume reduce the overall bilayer tension by 2 orders of magnitude, thereby producing tensionless bilayers. In addition, we show how to determine, for a certain total number of lipids, the unique spherical vesicle for which both leaflet tensions vanish individually. We also compute the local spontaneous curvature of the spherical membranes by identifying the first moment of the spherically symmetric stress profiles across the lipid bilayers with the nanoscopic torque as derived from curvature elasticity. Our study can be extended to other types of lipid membranes and sheds new light on cellular nanovesicles such as exosomes, which are increasingly used as biomarkers and drug delivery systems.

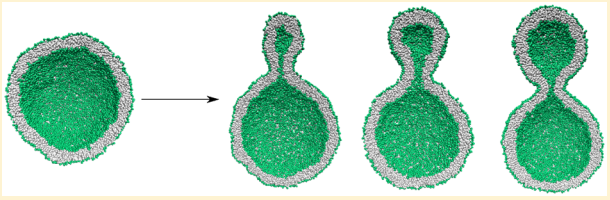

**KEYWORDS:** *Lipid bilayer, vesicle assembly, area per lipid, bilayer tension, leaflet tension, exosome*

Biomembranes are based on fluid bilayers of lipid molecules. The lipids are assembled into two leaflets, with the polar head groups of the lipids pointing toward the surrounding aqueous solutions and the hydrocarbon chains forming the hydrophobic core of the bilayer. The fluidity allows these membranes to respond to changes in their aqueous environment by fast remodelling of both their molecular composition and their shape. To avoid a hydrophobic edge, a single bilayer, which has a thickness of about 4 nm, closes up into a unilamellar vesicle, thereby separating an interior aqueous compartment from the exterior bulk solution. The size of these vesicles varies over a wide range, from a few tens of nanometers to hundreds of micrometers. This size range applies both to synthetic lipid vesicles prepared from a small number of lipid components and to cellular vesicles that involve a complex assortment of lipids and membrane proteins.

For lipid vesicles, a variety of methods have been developed by which one can prepare nanovesicles with diameters within the range 50−300 nm. These methods include extrusion of lipid dispersions through filters with a certain pore size[1,2] and, more recently, microfluidic mixing.[3] In vivo, even smaller nanovesicles are frequently observed such as synaptic vesicles with a diameter that varies between 20 and 50 nm[4,5] as well as exosomes, which represent small extracellular vesicles with a diameter between 25 and 100 nm.[6−8] In recent years, exosomes and somewhat larger extracellular vesicles have been intensely studied as possible biomarkers for diseases and as targeted drug delivery systems.[9−12]

The shapes of nanovesicles with a diameter below a few hundred nanometers, corresponding to the resolution limit of conventional optical microscopy, can be studied by variants of electron microscopy (EM) such as negative staining EM and cryo-EM.[13] Using such imaging methods, one often observes spherical nanovesicles, but a variety of nonspherical shapes have also been reported.[14−18] All EM methods are, however, restricted to a single snapshot of each nanovesicle and cannot monitor the time-dependent behavior of individual vesicles.

In contrast, computer simulations with molecular resolution can reveal the nanoscale dynamics of lipids and bilayer membranes as has been demonstrated, e.g., for the self-assembly of lipid bilayers in aqueous solution[19,20] or for the closure of bilayer patches into nanovesicles.[21] Here, we show that such simulations can also be used to monitor the shape transformations of individual nanovesicles, using the following simulation protocol. We first assembled spherical vesicles by placing $N_{il}$ and $N_{ol}$ lipid molecules onto two spherical shells,

**Received:** June 29, 2019
**Revised:** September 24, 2019
**Published:** September 26, 2019






DOI: 10.1021/acs.nanolett.9b02646
Nano Lett. 2019, 19, 7703−7711

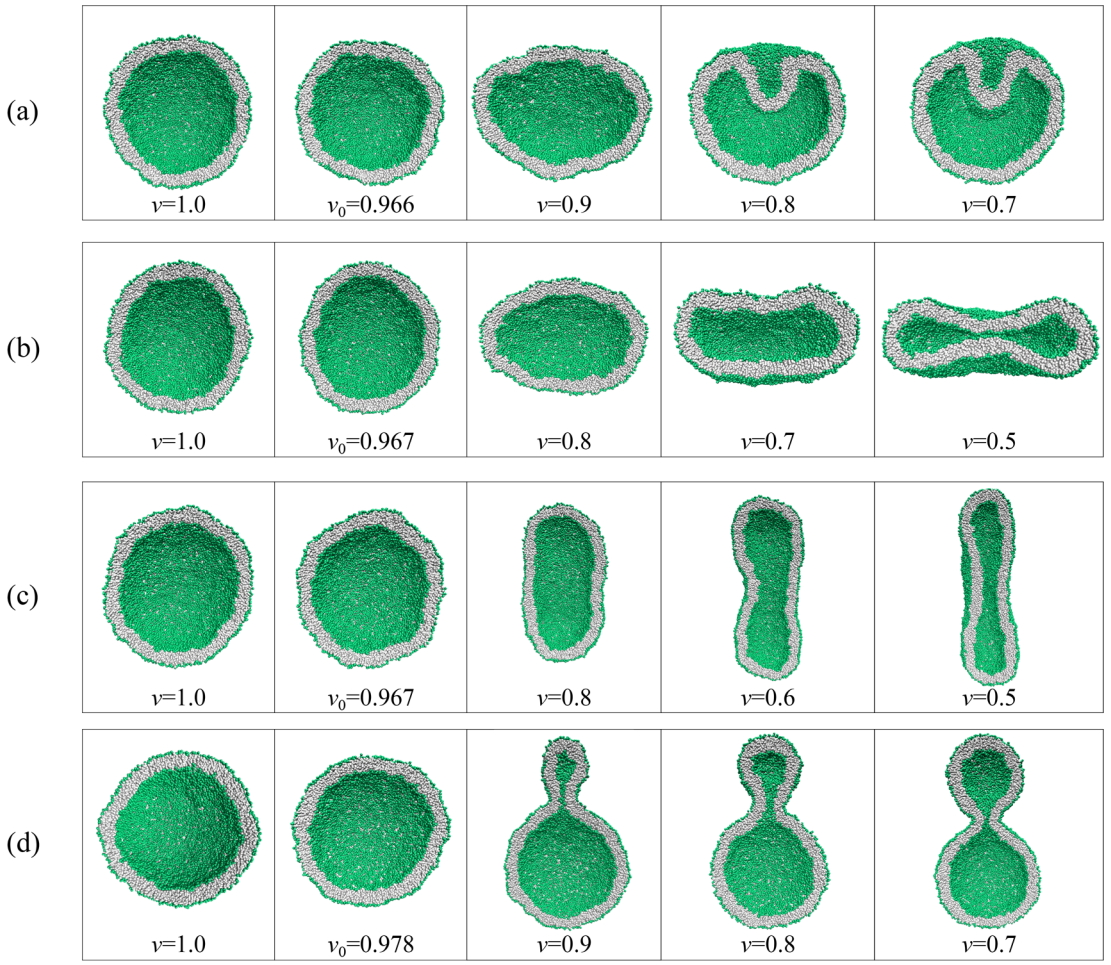


**Figure 1.** Distinct shape transformations of spherical nanovesicles in response to volume reduction: Each panel a–d displays a series of shapes that an individual vesicle attains when we decrease its volume as measured by the volume parameter $v$, see eq 1. In all four cases, we started from a spherical vesicle (leftmost snapshot, $v = 1$) that enclosed the same volume of water. In addition, the lipid bilayer of these vesicles contained the same total lipid number $N_{lip} = 10\,100$. However, the spherical vesicles differed slightly in the lipid numbers $N_{ol}$ and $N_{il} = N_{lip} - N_{ol}$, within their inner and outer leaflets. We first reduced the vesicle volume by a few percent to $v = v_0 < 1$ to decrease the bilayer tension by 2 orders of magnitude and to obtain a spherical vesicle with a tensionless bilayer. A further reduction of volume then led to (a) a stomatocyte for $N_{ol} = 5700$; (b) a discocyte for $N_{ol} = 5900$; (c) a tubelike prolate for $N_{ol} = 6100$; as well as (d) a dumbbell with a closed membrane neck for $N_{ol} = 6300$. Thus, redistributing only 200 lipids, i.e., less than 2% of the total lipid number $N_{lip}$, from the inner to the outer leaflets leads to qualitatively different shape transformations. As shown below, this polymorphism can be understood in terms of different mechanical tensions within the inner and outer leaflets of the spherical vesicles. The shape transformations in panels a and d are shown in more detail in Movies S1 and S2.

thereby constructing the inner and outer leaflets, respectively. The assembled vesicles enclosed a certain number $N_w^{isp}$ of water beads which defined the initial vesicle volume. For a given volume, we studied spherical vesicles which contained the same total number of lipids, $N_{lip}$, but slightly different lipid numbers $N_{ol}$ and $N_{il} = N_{lip} - N_{ol}$ within the inner and outer bilayer leaflets. Four such vesicles are displayed in the leftmost column of Figure 1a–d, corresponding to volume parameter $v = 1$.

When we reduced the volume of the spherical vesicles, thereby mimicking the experimental procedure of osmotic deflation, the vesicles underwent very different shape transformations as shown in Figure 1a–d. In fact, redistributing only 2% of the lipids between the two leaflets of the spherical vesicle led to a very different sequence of vesicle shapes. In this way, we directly demonstrate that molecular simulations provide a powerful method to explore the polymorphism of nanovesicles in a systematic manner by adjusting only three control parameters: the vesicle volume, the total number $N_{lip}$ of lipids assembled in the bilayer, as well as the lipid number $N_{ol}$ or $N_{il} = N_{lip} - N_{ol}$ within one of the two leaflets. As demonstrated by two movies in the Supporting Information, this simulation method also enables us to monitor the time-dependent behavior of individual vesicles. Therefore, our simulations provide unprecedented insights into the shape transformations of nanovesicles, which have not been accessible, so far, to experimental studies.

The vesicle volume and the lipid numbers represent *global* control parameters that can be directly adjusted in the simulations but do not reveal the physical mechanisms and driving forces that lead to the different shape transformations. These mechanisms and forces can be understood in terms of *local* quantities, as provided by the mechanical tensions within the two leaflets and the associated dilations of the molecular areas per lipid. In order to measure these leaflet tensions and area dilations, it is necessary to determine, for a given vesicle volume and total lipid number $N_{lip}$, the unique lipid number



DOI: 10.1021/acs.nanolett.9b02646
*Nano Lett.* 2019, 19, 7703–7711

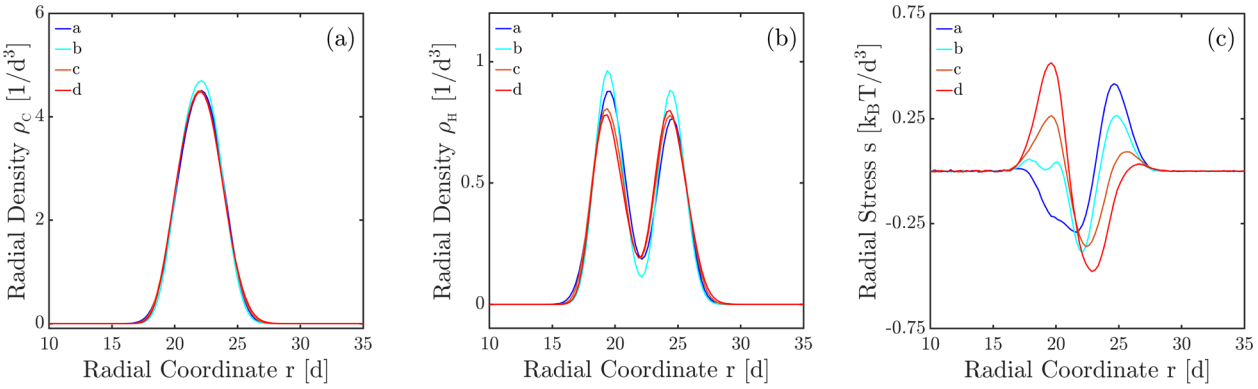


**Figure 2.** Density and stress profiles as functions of the radial coordinate $r$ for four spherical vesicles with tensionless bilayers corresponding to $v = v_0 < 1$ in Figure 1: (a) Density profiles $\rho_C(r)$ of the chain (C) beads forming the hydrophobic core of the bilayers. These profiles exhibit a pronounced maximum that is located at the radial coordinate $r = 22d$ and is used to define the midsurface of the bilayers. (b) Density profiles $\rho_H(r)$ of the head (H) beads that form the two headgroup layers of the bilayers. These density profiles have two peaks which we take to define the locations of the headgroup layers. (c) Stress profiles $s(r)$ with maxima and minima corresponding to stretched and compressed leaflets, respectively.

$N_{ol}^*$ for which both leaflet tensions vanish simultaneously within the spherical bilayer.

The shapes and shape transformations obtained here by molecular simulations of nanovesicles are qualitatively similar to those seen by optical microscopy of giant vesicles, which have a typical size of tens of $\mu$m and are, thus, 3 orders of magnitude larger than the nanovesicles in Figure 1. Our understanding of giant vesicle behavior is based on the theoretical framework of curvature elasticity.[22−25] Within this framework, one key parameter that determines the vesicle shape is the local spontaneous curvature. As shown at the end of this paper, the latter curvature can be related to the first moment of the spherically symmetric stress profile across the molecular bilayers.

Our Letter is organized as follows. We first describe the morphological responses of spherical nanovesicles to volume reduction and define the three parameters that determine the initial assembly of the spherical vesicle. We then compute the lipid areas in the two leaflets which are typically different, with the outer leaflet being more densely packed than the inner leaflet. Subsequently, we consider the stretching and compression of the bilayer leaflets and compute the individual leaflet tensions. We show that rather small changes in the vesicle volume reduce the overall bilayer tension by 2 orders of magnitude, thereby producing tensionless bilayers. These tensionless bilayers are characterized by nonzero leaflet tensions that change under the redistribution of the lipids between the two leaflets. We then identify the unique lipid distribution for which both leaflets of the vesicle membrane experience the same leaflet tension. When we reduce the volume of this vesicle, we obtain tensionless leaflets which define our unique reference state. At the end, we summarize our results and provide a short outlook on possible extensions and related systems to be addressed in future studies.

**Results and Discussion.** *Initial Assembly of Spherical Vesicles.* We consider closed nanovesicles formed by lipid bilayers in water and study their behavior by dissipative particle dynamics, see the Methods section for technical details. We use a coarse-grained model for the lipid and water molecules,[26,27] which are built up from beads with diameter $d \simeq 0.8$ nm. We first assembled spherical vesicles by placing lipid molecules onto two spherical shells corresponding to the two leaflets of the bilayer membranes. The size of these vesicles was primarily determined by the vesicle volume, i.e., by the number of water beads enclosed by the inner leaflet of the membrane. This number was chosen in such a way that the headgroup layers of the inner and outer leaflets had a diameter of about $45d$ and $50d$, respectively. For a given volume, we placed $N_{il}$ and $N_{ol}$ lipids onto the inner and outer leaflets, respectively, and considered different vesicles with the same total lipid number $N_{lip} = N_{il} + N_{ol}$. Thus, for given volume and constant total lipid number, we are left with a single assembly parameter, which we took to be the lipid number $N_{ol}$ in the outer leaflet. The spherical vesicles assembled in this manner were found to be stable for the range of $N_{ol}$-values shown in Figure 1.

*Vesicle Volume and Volume Parameter.* Experimentally, the volume of a vesicle can be changed by osmotic deflation and inflation. In the simulations, we varied the vesicle volume by changing the number $N_w$ of water beads enclosed by the inner leaflet of the vesicle membrane. This number determines the volume via $V \equiv N_w d^3/3$ where the factor 1/3 reflects the bulk water density $\rho_w = 3/d^3$. To monitor the volume changes, we used the volume parameter $v$ defined by

$$v \equiv \frac{N_w}{N_w^{isp}} \tag{1}$$

where $N_w^{isp}$ is the number of water beads enclosed by the initial spherical vesicle. Thus, the initial vesicle is characterized by $v = 1$, and any volume reduction with $N_w < N_w^{isp}$ leads to $v < 1$. Monitoring volume changes via the parameter $v$ is rather convenient here because we can directly change the number $N_w$ of water beads within the vesicle and thus compute the value of $v$ without the necessity to determine any membrane surface, see Figure 1.

*Diverse Morphological Responses to Volume Changes.* As we reduce the vesicle volume of a spherical nanovesicle, the vesicle can undergo a surprising variety of morphological transformations. In Figure 1, we display the morphological responses of four spherical vesicles that have the same volume, corresponding to $N_w^{isp} = 90\,400$ water beads, and are bounded by bilayer membranes that contain the same overall number of lipids as given by $N_{lip} = 10\,100$. However, the two leaflets of the bilayers contain somewhat different lipid numbers, $N_{ol}$ and $N_{il}$, within their outer and inner leaflets.



DOI: 10.1021/acs.nanolett.9b02646
Nano Lett. 2019, 19, 7703−7711

The diverse responses of the spherical nanovesicles in Figure 1 can be understood by examining how the different lipid numbers $N_{il}$ and $N_{ol}$ change the areas per lipid in the two leaflets of the bilayers. Indeed, when we place, for fixed vesicle volume, somewhat different numbers of lipids on the inner and outer leaflets of the spherical bilayers, we obtain different molecular areas, $a_{il}$ and $a_{ol}$, for the lipids in the two bilayer leaflets.

*Lipid Areas in the Two Leaflets.* To determine the two lipid areas $a_{il}$ and $a_{ol}$ in a quantitative manner, we introduce spherical coordinates with the radial coordinate $r$ and place the center of each spherical vesicle at $r = 0$. Because of the spherical symmetry, all density profiles depend only on this radial coordinate. We then define the midsurface of each spherical nanovesicle via the corresponding density profile $\rho_C(r)$ of the chain (C) beads that form the hydrophobic core of the vesicle membranes. As shown in Figure 2a, this density profile exhibits a pronounced maximum at $r = R_C = 22d$ by which we define the radius $R_{mid}$ of the bilayer's midsurface, as in previous studies[26,27] of planar bilayers. In contrast to the neutral surface of a bilayer,[28,29] the midsurface considered here is not defined in terms of elastic deformations or stresses but represents the molecular interface between the two bilayer leaflets. Furthermore, as shown further below and summarized in Table S3, three alternative, physically meaningful definitions of this midsurface lead to essentially the same numerical value for the midsurface radius $R_{mid}$. In addition to the density profiles $\rho_C$, we consider the density profiles $\rho_H(r)$ of the head (H) beads, see Figure 2b, which exhibit two peaks at $r = R_{iH}$ for the inner headgroup layer and at $r = R_{oH}$ for the outer one. The midsurface of the inner leaflet is then defined by $R_{il} \equiv \frac{1}{2}(R_{iH} + R_C)$ and the midsurface of the outer leaflet by $R_{ol} \equiv \frac{1}{2}(R_C + R_{oH})$. Finally, the lipid areas in the inner and outer leaflets are obtained by dividing the areas of the leaflets' midsurfaces by the corresponding lipid numbers, i.e., by

$$a_{il} = \frac{4\pi R_{il}^2}{N_{il}} \quad \text{and} \quad a_{ol} = \frac{4\pi R_{ol}^2}{N_{ol}} \tag{2}$$

The numerical values of these lipid areas as obtained for the four spherical vesicles with $v = 1$ in Figure 1 are given in Table S1. In all cases, the lipid area $a_{il}$ within the inner leaflet is larger than the lipid area $a_{ol}$ within the outer leaflet which implies that the outer leaflets are more densely packed.

*Stretching and Compression of the Bilayer Leaflets.* Intuitively, we expect that the inner and the outer leaflet of the vesicle membrane have an optimal area per lipid, $a_{il}^0$ and $a_{ol}^0$, corresponding to their natural packing densities and their elastically relaxed states. Let us assume, for a moment, that we knew these optimal lipid areas. If we now stretched the outer leaflet of the spherical bilayer, we would increase the lipid area to $a_{ol} > a_{ol}^0$. On the other hand, if we compressed the outer leaflet, we would reduce this lipid area to $a_{ol} < a_{ol}^0$. The same behavior applies to the inner leaflet of the spherical bilayer: $a_{il} < a_{il}^0$ corresponds to compression, and $a_{il} > a_{il}^0$ corresponds to stretching of the inner leaflet.

To determine the optimal lipid areas $a_{il}^0$ and $a_{ol}^0$, we need to know the mechanical tensions, $\Sigma_{il}$ and $\Sigma_{ol}$, that act within the inner and outer leaflets. These leaflet tensions were computed as follows. Because of the spherical symmetry, the local stress or pressure tensor has the general form[30]

$$\mathbf{P} = P_N(r)\mathbf{e}_r \otimes \mathbf{e}_r + P_T(r)[\mathbf{e}_\theta \otimes \mathbf{e}_\theta + \mathbf{e}_\phi \otimes \mathbf{e}_\phi] \tag{3}$$

with the normal component $P_N(r)$ and the tangential component $P_T(r)$ where $\mathbf{e}_r$, $\mathbf{e}_\theta$, and $\mathbf{e}_\phi$ are orthogonal unit vectors, and the symbol $\otimes$ represents the dyadic product. The numerical values of $P_N(r)$ and $P_T(r)$ as well as the stress profile $s(r) \equiv P_N(r) - P_T(r)$ were calculated as described previously.[31,32] As shown in Figure 2c, the stress profiles $s(r)$ change strongly as we reshuffle lipids from one leaflet to the other, thereby changing the lipid numbers $N_{ol}$ and $N_{il} = N_{lip} - N_{ol}$. The bilayer tension $\Sigma$ was obtained by

$$\Sigma = \int_0^\infty dr\, [P_N(r) - P_T(r)] = \int_0^\infty dr\, s(r) \tag{4}$$

in close analogy to the interfacial tension[30] of a spherical liquid droplet, and the leaflet tensions $\Sigma_{il}$ and $\Sigma_{ol}$ by

$$\Sigma_{il} = \int_0^{R_C} dr\, s(r) \quad \text{and} \quad \Sigma_{ol} = \int_{R_C}^\infty dr\, s(r) \tag{5}$$

In this way, we obtained the numerical values of the bilayer tension $\Sigma = \Sigma_{il} + \Sigma_{ol}$ and the leaflet tensions for the four spherical vesicles in Figure 1, see Table S1 for $v = 1$.

*Leaflet Tensions of Spherical Bilayers.* The first column in Table S1 corresponds to the spherical vesicle displayed in Figure 1a with $N_{il} = 4400$, $N_{ol} = 5700$, and $N_w^{isp} = 90\,400$. In this case, the tension $\Sigma_{ol}$ of the outer leaflet is positive whereas the tension $\Sigma_{il}$ of the inner leaflet is negative. Thus, the outer leaflet is stretched whereas the inner leaflet is compressed. Furthermore, the overall bilayer tension $\Sigma$ is quite substantial with a value of about $0.34k_BT/d^2$. The first column of Table S2 provides the tension values obtained after a slight reduction of the vesicle volume from $N_w^{isp} = 90\,400$ to $N_w = 87\,350$ water beads. For the latter volume, the slightly deflated vesicle attained a state for which the overall bilayer tension $\Sigma$ was reduced by 2 orders of magnitude, from $\Sigma \simeq 0.34k_BT/d^2$ to $\Sigma = 0.05k_BT/d^2$, corresponding to a tensionless bilayer.

However, the two leaflet tensions $\Sigma_{il} \simeq -0.82$ and $\Sigma_{ol} \simeq 0.87$ were still comparable with the leaflet tensions of the initial vesicle that enclosed $N_w^{isp} = 90\,400$ water beads, corresponding to an inner leaflet that is compressed and an outer leaflet that is stretched. Therefore, when we further reduce the volume of the vesicle, the inner leaflet would like to expand whereas the outer leaflet would like to shrink, thereby reducing the area difference $\Delta A = A_{ol} - A_{il}$ between the outer and the inner leaflet. As a consequence, the spherical vesicle in Figure 1a is transformed into a stomatocyte which has a smaller area difference $\Delta A$ than the spherical vesicle.

Inspection of Table S1 shows that analogous results are obtained for the other three spherical vesicles with $v = 1$ in Figure 1b–d. For the spherical vesicle in Figure 1b, the tension $\Sigma_{il}$ of the inner leaflet is again negative whereas the tension $\Sigma_{ol}$ is again positive, but these tensions are reduced compared to the spherical vesicle in Figure 1a. Thus, the inner leaflet is again compressed while the outer leaflet is again stretched. In contrast, for the spherical vesicles in Figure 1c,d, the inner leaflet tension $\Sigma_{il}$ is positive while the outer leaflet tension $\Sigma_{ol}$ is negative. Therefore, the inner leaflets are stretched and would like to shrink whereas the outer leaflets are compressed and would like to expand, thereby increasing the area difference $\Delta A$. As a consequence, the spherical vesicles in Figure 1c,d transform into prolates and dumbbells, which have larger $\Delta A$-values than the spherical vesicles.



DOI: 10.1021/acs.nanolett.9b02646
Nano Lett. 2019, 19, 7703−7711

To facilitate the comparison between the different spherical vesicles in Figure 1a–d, we always started from an initial volume with $N_w^{isp}$ = 90 400 water beads. In all four cases, we had to reduce the initial spherical nanovesicles with $v = 1$ by a few percent to $v = v_0 < 1$, see second column of Figure 1 and Table S2, in order to reach a tensionless bilayer, corresponding to $\Sigma = \Sigma_{il} + \Sigma_{ol} \simeq 0$. The slightly deflated vesicles with $v = v_0 < 1$ and $\Sigma \simeq 0$ are still spherical, and their snapshots cannot be distinguished from those for $v = 1$, see Figure 1.

*Reference State with Tensionless Leaflets.* The four vesicles with $v = 1$ in Figure 1 were obtained by assembling different lipid numbers $N_{il}$ and $N_{ol}$ in the two leaflets, keeping the total lipid number $N = N_{il} + N_{ol}$ fixed. We can then reduce the number of parameters and focus on a single lipid number, say $N_{ol}$. In Figure 3, we display the two leaflets tensions $\Sigma_{il}$ and $\Sigma_{ol}$ as functions of the lipid number $N_{ol}$. The two sets of data points in this figure are well-fitted by two straight lines that cross each other for $N_{ol} = N_{ol}^* = 5963$. At this crossing point, the two leaflet tensions are equal to $\Sigma_{il} = \Sigma_{ol} \simeq 0.16 k_B T/d^2$.

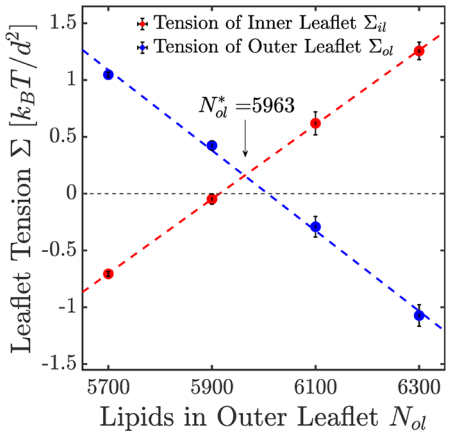


**Figure 3.** Leaflet tensions $\Sigma_{il}$ (red) and $\Sigma_{ol}$ (blue) as functions of the lipid number $N_{ol}$ in the outer leaflet for the four spherical vesicles displayed in Figure 1 with fixed total number $N = N_{il} + N_{ol}$ = 10 100 and volume parameter $v = 1$. The tension $\Sigma_{il}$ in the inner leaflet increases whereas the tension $\Sigma_{ol}$ in the outer leaflet decreases with increasing $N_{ol}$. Furthermore, both sets of data are well-fitted by straight lines which cross at $N_{ol}^* = 5963$, corresponding to equal leaflet tensions $\Sigma_{il} = \Sigma_{ol} \simeq 0.16 k_B T/d^2$.

We then studied a spherical vesicle with $N_{ol} = N_{ol}^*$ and $N_{il} = N_{il}^* = N_{lip} - N_{ol}^*$, see Figure 4a, that encloses the same number of beads, $N_w^{isp}$ = 90 400, as the four spherical vesicles in Figure 1. As a result, we obtained the leaflet tensions $\Sigma_{il} = (0.157 \pm 0.07) k_B T/d^2$ and $\Sigma_{ol} = 0.209 \pm 0.06$, in good agreement with the tension values $\Sigma_{il} = \Sigma_{ol} \simeq 0.16 k_B T/d^2$ as derived from the graphical interpolation in Figure 3. When we slightly deflated this vesicle and reduced its volume to $N_w$ = 87 360, we obtained a spherical vesicle for which both leaflet tensions $\Sigma_{ol} \simeq 0$ and $\Sigma_{il} \simeq 0$, i.e., for which each leaflet tension vanished individually, see Table S2. As explained in the Supporting Information and displayed in Figure S1, this reference state can also be reached by an alternative procedure in which we swap the deflation and graphical interpolation steps. The reference state with tensionless leaflets has the reduced volume $v = v_0$ = 0.966 as well as the lipid areas, $a_{ol}^0 = 1.139 d^2$ and $a_{il}^0 = 1.318 d^2$, corresponding to optimal packing densities within the outer and inner leaflets of the bilayer membrane. As shown in Figure 4a, a further reduction of the volume leads to prolates and discocytes.

For planar membranes, the reference state is provided by a symmetric and tensionless bilayer. In this case, both leaflets contain the same number of lipids, $N_{ol} = N_{il}$, have the same area per lipid, $a_{ol} = a_{il}$, and have the same leaflet tension, $\Sigma_{ol} = \Sigma_{il}$. Furthermore, if the bilayer is tensionless with $\Sigma_{il} + \Sigma_{ol} = 0$, it directly follows that both leaflet tensions vanish, and $\Sigma = \Sigma_{il} = \Sigma_{ol} = 0$.[26] In contrast, for the spherical nanovesicles considered here, the reference state with tensionless leaflets $\Sigma_{il} = \Sigma_{ol} = 0$ is characterized by $N_{il} < N_{ol}$ and $a_{il}^0 > a_{ol}^0$, see Table S2.

*Area Compressibility Moduli of Two Leaflets.* The deviations of the lipid areas from their optimal values for the reference state are related to the leaflet tensions $\Sigma_{il}$ and $\Sigma_{ol}$ according to

$$\Sigma_{il} \approx K_{il} \Delta_{il} \quad \text{with} \quad \Delta_{il} \equiv \frac{a_{il} - a_{il}^0}{a_{il}^0} \tag{6}$$

and

$$\Sigma_{ol} \approx K_{ol} \Delta_{ol} \quad \text{with} \quad \Delta_{ol} \equiv \frac{a_{ol} - a_{ol}^0}{a_{ol}^0} \tag{7}$$

for small area dilations $\Delta_{il}$ and $\Delta_{ol}$ where $K_{il}$ and $K_{ol}$ represent the area compressibility moduli of the two leaflets. The corresponding data for leaflet tensions and dimensionless area deviations $\Delta_{il}$ and $\Delta_{ol}$ are plotted in Figure 5a for the five vesicle membranes whose bilayer tension $\Sigma = \Sigma_{ol} + \Sigma_{il} \simeq 0$, see also Table S2. Inspection of this figure shows that these data are well-fitted, for the whole range of $\Delta$-values studied here, by straight lines with the area compressibility moduli $K_{il} = 13.9 k_B T/d^2$ and $K_{ol} = 15.9 k_B T/d^2$. Therefore, the inner leaflet is found to be more compressible and softer than the outer leaflet. This result is consistent with the lipid areas $a_{il}^0 = 1.31 d^2$ and $a_{ol}^0 = 1.14 d^2$ for the two tensionless leaflets (Table S2). Indeed, the more loosely packed inner leaflet is expected to be softer than the more densely packed outer leaflets.

*Alternative Definitions of the Bilayer's Midsurface.* The numerical results described so far were obtained by locating the bilayer's midsurface at the peak position $r = R_C$ of the C bead density $\rho_C(r)$, see Figure 2a, and to define the midsurface radius via $R_{mid} \equiv R_C$, a definition that we now denote as CHAIN. We also explored two alternative, physically meaningful definitions of the midsurface radius. One alternative definition, HEAD, was based on the two peaks of the density profile $\rho_H(r)$ for the headgroup layers, see Figure 2b, and on the corresponding radii $r = R_{iH}$ and $r = R_{oH}$. The midsurface radius was then defined by $R_{mid} = R_H \equiv \frac{1}{2}(R_{iH} + R_{oH})$. A second alternative definition, COM, used the center-of-mass radius $R_{COM}$ of the combined density profile $\rho_C(r) + \rho_H(r)$ and defined the midsurface radius by $R_{mid} \equiv R_{COM}$.

Using these three definitions of the midsurface radius, we obtained the numerical values in Table S3 for the five spherical vesicles in Figures 1 and 4 with $v = v_0$, corresponding to tensionless bilayers. Inspection of this table shows that, for each vesicle, the three values $R_C$, $R_H$, and $R_{COM}$ obtained for the midsurface radius $R_{mid}$ were rather close and differed by at most 3%. Likewise, using COM, we also find different area compressibilities $K_{il}$ and $K_{ol}$ for the inner and outer leaflets, see Figure S3, in agreement with the CHAIN results shown in Figure 5a.



DOI: 10.1021/acs.nanolett.9b02646
*Nano Lett.* 2019, 19, 7703–7711

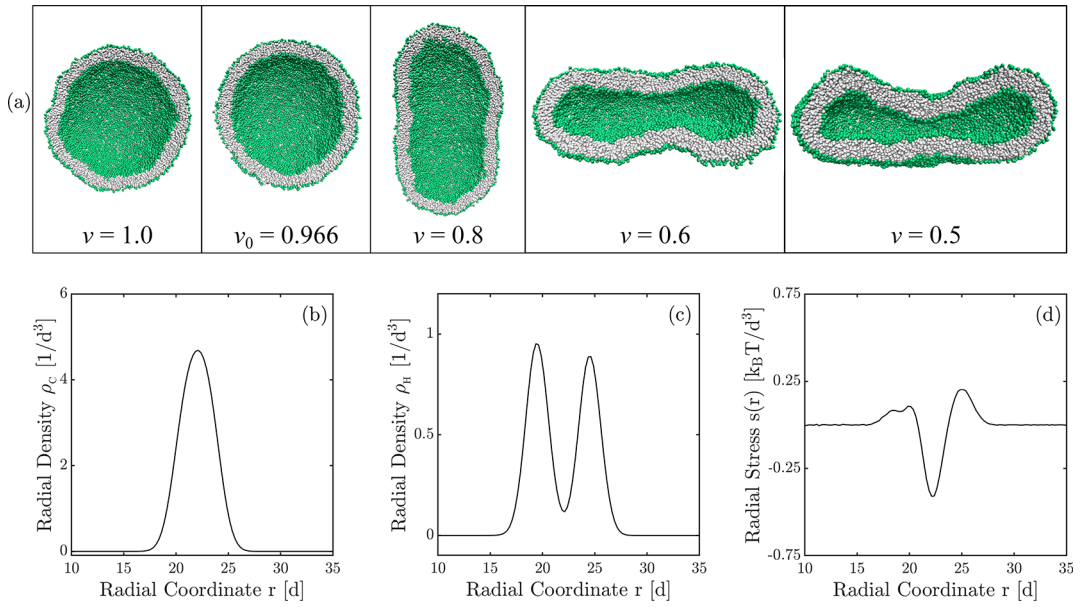


**Figure 4.** (a) Morphological transformations of the spherical nanovesicle with $N_{il}$ = 4137 and $N_{ol}$ = 5963 lipids in the inner and outer leaflet, enclosing $N_w^{isp}$ = 90 400 water beads. A slight deflation of this vesicle to $N_w$ = 87 360 water beads and $v = v_0$ = 0.966 leads to the reference state with tensionless leaflets. As we continue to reduce the vesicle volume, the vesicle attains a prolate shape for $v$ = 0.8 and $v$ = 0.7, an oblate or discocyte shape for $v$ = 0.6, and a stomatocyte shape for $v$ = 0.5. (b–d) Density and stress profiles of the reference state with tensionless leaflets as functions of the radial coordinate $r$: (b) density profile $\rho_C(r)$ of the C beads; (c) density profile $\rho_H(r)$ of the H beads; and (d) stress profile $s(r)$ across the bilayer membrane. Integrating this stress profile over the two leaflets as in eq 5, we obtain leaflet tensions $\Sigma_{il}$ and $\Sigma_{ol}$ close to zero (Table S2).

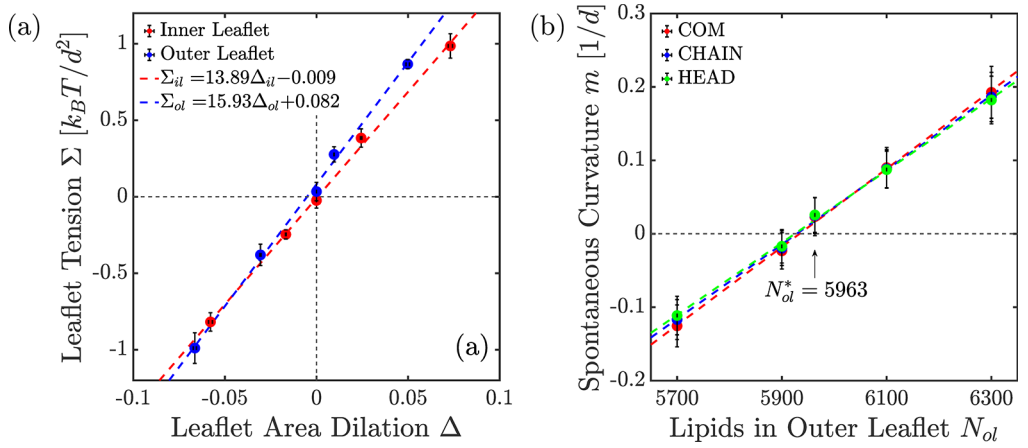


**Figure 5.** (a) Leaflet tension $\Sigma_{il}$ (red) and $\Sigma_{ol}$ (blue) as a function of the dimensionless area dilations $\Delta_{il}$ and $\Delta_{ol}$, defined in eqs 6 and 7. The straight lines represent least-squares fits which determine the area compressibility modulus $K_{il} = 13.89 k_BT/d^2$ and $K_{ol} = 15.93 k_BT/d^2$ for the inner and outer leaflet, respectively. These results were obtained using the CHAIN definition for the bilayer's midsurface. (b) Local spontaneous curvature $m$ versus lipid number $N_{ol}$ in the outer leaflet, as obtained from eq 8 for bending rigidity $\kappa = 15 k_BT$ and three alternative definitions (CHAIN, HEAD, and COM) of the midsurface radius $R_{mid}$.

*Local and Nonlocal Spontaneous Curvature.* The shapes and shape transformations of nanovesicles as observed in our molecular simulations, see Figure 1, are qualitatively similar to those obtained from curvature models.[22−25] In these models, the vesicle membranes are viewed as smooth surfaces, and their behavior is described in terms of a few fluid-elastic parameters such as the bending rigidity $\kappa$ and the local spontaneous curvature $m$. In fact, as far as vesicle shapes are concerned, the most important fluid-elastic parameter is the spontaneous curvature. For planar bilayers, this curvature can be computed by identifying the microscopic torque across the molecular bilayer with the nanoscopic torque as obtained from curvature elasticity.[26,33] As shown in the Supporting Information, the latter approach can be extended to spherical vesicles, using the corresponding nanoscopic torques,[34,35] which leads to the relationship

$$2\kappa\left(\frac{1}{R_{mid}} - m\right) = \int_0^\infty dr\, s(r) r \tag{8}$$

between the bending rigidity $\kappa$, the midsurface radius $R_{mid}$ of the spherical vesicle, the spontaneous curvature $m$, and the first moment of the stress profile $s(r)$.

The magnitude of the bending rigidity $\kappa$ can be obtained from the area compressibility modulus $K_A$ of the bilayer using the relationship $\kappa = K_A l_{me}^{\ 2}/48$ which provides the same $\kappa$-value as the computationally more expensive fluctuation analysis.[27,36] For the vesicle membranes in Figure 1, the area



DOI: 10.1021/acs.nanolett.9b02646
Nano Lett. 2019, 19, 7703−7711

compressibility $K_A = K_{il} + K_{ol} \simeq 30k_BT$ and the membrane thickness $l_{me} \simeq 5d$ which leads to $\kappa \simeq 15k_BT$. Using this $\kappa$-value in eq 8, together with the $R_{mid}$-values in Table S3 and the numerical values for the first moment $\mathcal{T}$ of the stress profile in Figure S2 and Table S2, we obtain the values of the local spontaneous curvature $m$ as shown in Figure 5b. Inspection of this figure reveals that $m$ increases linearly with the lipid number $N_{ol}$ in the outer leaflet and that all three definitions, CHAIN, HEAD, and COM, of the midsurface radius $R_{mid}$ lead to very similar values for the spontaneous curvature $m$, in accordance with the $R_{mid}$-values in Table S3.

In the absence of flip-flops between the two leaflets, the theory of curvature elasticity predicts another nonlocal contribution to the spontaneous curvature[25,37] arising from area-difference-elasticity,[23,24] which depends on the difference $\Delta A = A_{ol} - A_{il}$ between the outer leaflet area $A_{ol}$ and the inner leaflet area $A_{il}$. This nonlocal contribution to the spontaneous curvature is proportional to the deviation of $\Delta A$ from its reference value $\Delta A_0$ for tensionless leaflets. However, the four spherical vesicles in Figure 1, corresponding to $v = v_0$ and tensionless bilayers, have practically the same midsurface radius $R_{mid}$, see Table S3, and thus the same area difference as the relaxed vesicle in Figure 4a with $v = v_0$. Therefore, for these vesicle shapes, the nonlocal contribution to the spontaneous curvature is very small and can be ignored. On the other hand, once the nanovesicles have attained strongly nonspherical shapes, area-difference-elasticity should make a significant contribution, which is, however, difficult to determine quantitatively because it is shape-dependent and involves another elastic modulus.

**Summary and Outlook.** In summary, we showed that spherical nanovesicles can transform into a multitude of nonspherical shapes as illustrated in Figures 1 and 4. This polymorphism which involves a large variety of different shapes—prolates, oblates, discocytes, stomatocytes, and dumbbells—has been obtained here by reducing the vesicle volume for a fixed total number of lipids and for a fixed distribution of the lipid molecules between the two leaflets. Alternatively, we may also consider a fixed volume and shuffle some lipids from the inner to the outer leaflet, thereby moving from panels a and b of Figure 1 via Figure 4 to panels c and d of Figure 1. Experimentally, the latter morphological pathway could be induced by adding lipid or surfactant molecules to the exterior solution which then insert into the outer membrane leaflet and increase its area.

The different shapes displayed in Figures 1 and 4 arise from small changes in the assembly process of the spherical vesicles which leads to small variations of the number of lipid molecules within the two bilayer leaflets. The resulting shape transformations can be understood in terms of the individual leaflet tensions $\Sigma_{il}$ and $\Sigma_{ol}$, which act to stretch or compress these leaflets when we allow the vesicles to attain nonspherical shapes by reducing their volume. We also identified, for a given vesicle volume and total lipid number $N_{lip} = N_{il} + N_{ol}$, the unique reference state of the spherical vesicle for which both leaflets are tensionless with $\Sigma_{il} = \Sigma_{ol} = 0$ (Figures 3 and 4, and Figure S1.) Even for vanishing leaflet tensions, the two leaflets had different areas per lipid, $a_{il}^0 = 1.3d^2$ and $a_{il}^0 = 1.1d^2$ (Table S2), corresponding to a more loosely packed inner leaflet and a more densely packed outer leaflet.

To characterize the stress asymmetry of the spherical bilayer, we extended previous results on planar bilayers to obtain a simple relation between the radius of the midsurface, the (local) spontaneous curvature, and the first moment of the spherically symmetric stress profile (eq 8). The resulting spontaneous curvature was observed to increase linearly with the number of lipids assembled in the outer leaflet as shown in Figure 5b. Finally, we also argued that the nonlocal contribution to the spontaneous curvature arising from area-difference-elasticity can be ignored for spherical bilayers.

In the present paper, we focused on nanovesicles with a single lipid component and studied several distributions of lipid numbers $N_{il}$ and $N_{ol}$ within the two leaflets, keeping the total number $N = N_{il} + N_{ol}$ fixed (Figures 1 and 4, Tables S1−S6). As a consequence, we explored a certain range of leaflet tensions $\Sigma_{il}$ and $\Sigma_{ol}$ as depicted in Figures 3 and 5a. For this tension range, the lipids did not undergo flip-flops between the two leaflets over the time scales of our simulations, which were of the order of 50 $\mu$s. However, such lipid flip-flops are expected to occur if the lipid numbers $N_{il}$ and $N_{ol}$ become sufficiently different and the resulting leaflet tensions sufficiently large. An interesting objective for future studies is to determine the corresponding threshold values for the leaflet tensions. A related problem is the relaxation of multicomponent bilayers that contain (at least) one lipid component such as cholesterol that undergoes frequent flip-flops even for relatively small leaflet tensions. For planar bilayers, it has been recently shown that these flip-flops lead to bilayers with tensionless leaflets.[33]

One type of cellular nanovesicle that has attracted a lot of recent interest is provided by exosomes, small extracellular vesicles, which are increasingly investigated as biomarkers for diseases and as targeted drug delivery systems.[9−12] Exosomes are produced within late endosomes or multivesicular bodies by inward budding of the endosomal membrane and are released to the extracellular environment after fusion of the multivesicular bodies with the plasma membrane.[7,8] These nanovesicles have a specific lipid composition enriched in cholesterol[38,39] and can attain a variety of different morphologies,[10,40] including long tubelike shapes. Such shapes could be formed at various stages of the exosomes' biogenesis: already in the multivesicular bodies or during exocytosis or after release into the extracellular medium. One possibility is that these different environments impose different osmotic conditions on the vesicles. If these changing conditions lead to strong osmotic deflation of the exosomes, their morphology can be transformed from spheres to long tubelike prolates as in Figure 1c. Alternatively, the shape of extracellular vesicles could be molded by the activity of flippases which are present in their membranes[41,42] and translocate lipids from one leaflet to the other.

**Methods.** We used dissipative particle dynamics (DPD) which is a coarse-grained molecular dynamics simulation technique, well-suited to study nanoscale processes related to bilayer membranes. Our system is built up from three types of beads that represent small molecular groups corresponding to water (W) beads, lipid chain (C) beads, and lipid head (H) beads. The lipid molecules have a headgroup consisting of three H beads and two hydrocarbon chains, each of which consists of six C beads.[26,27] All beads have the diameter $d$, corresponding to about 0.8 nm. Each pair of beads interacts with short-ranged pairwise additive forces including the conservative force



DOI: 10.1021/acs.nanolett.9b02646
Nano Lett. 2019, 19, 7703−7711

$$\vec{F}_{ij}^{C} = f_{ij}(1 - r_{ij}/d)\hat{r}_{ij} \quad \text{for } r_{ij} < d$$
$$= 0 \quad \text{for } r_{ij} > d \tag{9}$$

with the force parameter $f_{ij}$, the unit vector $\hat{r}_{ij}$ pointing from bead $j$ to bead $i$, and the distance $r_{ij}$ between bead $i$ and bead $j$. The numerical values of the force parameters $f_{ij}$ are displayed in Table 1. More technical details about the DPD simulations can be found in refs 26 and 27.

**Table 1. Set of Force Parameters $f_{ij}$ in Units of $k_BT/d$[a]**

| | $f_{ij}$ | | |
|---|---|---|---|
| | $j$ = H | $j$ = C | $j$ = W |
| $i$ = H | 30 | 50 | 30 |
| $i$ = C | 50 | 10 | 75 |
| $i$ = W | 30 | 75 | 25 |

[a]The bead indices $i$ and $j$ can be H, C, or W. H denotes the lipid head beads, C the lipid chain beads, and W the water beads.

The bead diameter $d$ and the bead mass $m_{be}$ provide the basic length and mass scales in our simulations, whereas the basic energy unit is the thermal energy $k_BT$ with Boltzmann's constant $k_B$ and absolute temperature $T$. The basic time scale is $\tau = \sqrt{d^2 m_{be}/(k_BT)}$, which is of the order of 1 ns, and the time step for integrating the equations of motion was $\delta t = 0.01\tau$. For all simulations, we used LAMMPS (Large Scale Atomic/Molecular Massively Parallel Simulator), which is a highly efficient, parallelized classical molecular dynamics simulator.[43] All DPD simulations were performed in the NVT ensemble. The bulk water density was chosen to have the standard DPD value $\rho_w = 3/d^3$ to reproduce the compressibility of bulk water at room temperature $T$ = 298 K. The nanovesicles were studied in a cubic simulation box with volume $(80d)^3$ and periodic boundary conditions. The initial spherical nanovesicles were assembled on two nested spherical shells with diameter 45$d$ and 50$d$, using the packmol software package.[44] We placed $N_{il}$ and $N_{ol}$ lipids within the inner and outer shell and varied these lipid numbers in such a way that the total number $N = N_{il} + N_{ol}$ was kept constant, see Figure 1. For the initial spherical nanovesicles, the interior and exterior aqueous compartment contained 90 400 and 1 350 000 water beads, respectively. For each vesicle volume, the simulation run time was at least 50 $\mu$s.

## ■ ASSOCIATED CONTENT

### Supporting Information

The Supporting Information is available free of charge on the ACS Publications website at DOI: 10.1021/acs.nanolett.9b02646.

Alternative procedure to determine the reference state with tensionless leaflets, derivation of eq 8, movie captions, and additional data and figures including leaflet tension vs $N_{ol}$, first moment of stress profile vs $N_{ol}$, and leaflet tension vs leaflet area difference (PDF)

Movie S1: shape transformation of a nanovesicle with $N_{il}$ = 4400 and $N_{ol}$ = 5700 lipid molecules in the inner and outer leaflet of the vesicle membrane (AVI)

Movie S2: shape transformation of a nanovesicle with $N_{il}$ = 3800 and $N_{ol}$ = 6300 lipid molecules in the inner and outer leaflet of the vesicle membrane (AVI)

## ■ AUTHOR INFORMATION


### Corresponding Author

*E-mail: lipowsky@mpikg.mpg.de.

### ORCID

Andrea Grafmüller: 0000-0002-1671-3158

Reinhard Lipowsky: 0000-0001-8417-8567


### Author Contributions

†R.G. and V.S. contributed equally to this work.

### Notes

The authors declare no competing financial interest.

## ■ ACKNOWLEDGMENTS

This work was supported by the Max Planck Society and the German Federal Ministry of Education and Research (BMBF) via the MaxSynBio consortium as well as via the International Max Planck Research School on "Multiscale Bio-Systems".

## ■ REFERENCES


(1) Hope, M. J.; Bally, M. B.; Webb, G.; Cullis, P. R. Produciton of Large Unilamellar Vesicles by a Rapid Extrusion Procedure. Characterization of Size Dstribution, Trapped Volume and Ability to Maintain a Membrane Potential. *Biochim. Biophys. Acta, Biomembr.* **1985**, *812*, 55−65.

(2) MacDonald, R. C.; MacDonald, R. I.; Menco, B. P. M.; Takeshita, K.; Subbarao, N. K.; Hu, L.-R. Small-Volume Extrusion Apparatus for Preparation of Large Unilamellar Vesicles. *Biochim. Biophys. Acta, Biomembr.* **1991**, *1061*, 297−303.

(3) Jahn, A.; Stavis, S. M.; Hong, J. S.; Vreeland, W. N.; DeVoe, D. L.; Gaitan, M. Microfluidic Mixing and the Formation of Nanoscale Lipid Vesicles. *ACS Nano* **2010**, *4*, 2077−2087.

(4) Qu, L.; Akbergenova, Y.; Hu, Y.; Schikorski, T. Synpase-to-Synapse Variation in Mean Synaptic Vesicle Size and Its Relationship With Synamptic Morphology and Function. *J. Comp. Neurol.* **2009**, *514*, 343−352.

(5) Hopiavuori, B. R.; Bennett, L. D.; Brush, R. S.; Hook, M. J. V.; Thoreson, W. B.; Anderson, R. E. Very Long-Chain Fatty Acids Support Synaptic Structure and Function in the Mammalian Retina. *OCL: Oilseeds Fats, Crops Lipids* **2016**, *23*, D113.

(6) Johnstone, R. M.; Adam, M.; Hammond, J. R.; Orr, L.; Turbide, C. Vesicle Formation during Reticulocyte Maturation. *J. Biol. Chem.* **1987**, *262*, 9412−9420.

(7) Simons, M.; Raposo, G. Exosomes - Vesicular Carriers for Intercellular Communication. *Curr. Opin. Cell Biol.* **2009**, *21*, 575−581.

(8) Hanson, P. I.; Cashikar, A. Multivesicular Body Morphogenesis. *Annu. Rev. Cell Dev. Biol.* **2012**, *28*, 337−362.

(9) Barile, L.; Vassalli, G. Exosomes: Therapy Delivery Tools and Tiomarkers of Diseases. *Pharmacol. Ther.* **2017**, *174*, 63−78.

(10) Lässer, C.; Jang, S. C.; Lötvall, J. Subpopulations of Extracellular Vesicles and Their Therapeutic Potential. *Mol. Aspects Med.* **2018**, *60*, 1−14.

(11) Antimisiaris, S. G.; Mourtas, S.; Marazioti, A. Exosomes and Exosome-Inspired Vesicles for Targetet Drug Delivery. *Pharmaceutics* **2018**, *10*, 218.

(12) Han, L.; Lam, E. W.-F.; Sun, Y. Extracellular Vesicles in the Tumor Microenvironment: Old Stories, but New Tales. *Mol. Cancer* **2019**, *18*, 59.

(13) Baxa, U. In *Imaging of Liposomes by Transmission Electron Microscopy*; McNeil, S. E., Ed.; Springer Science+Business Media, 2018; Vol. *1682*.

(14) Mui, B. L.-S.; Cullis, P. R.; Evans, E. A.; Madden, T. D. Osmotic Properties of Large Unilamellar Vesicles Prepared by Extrusion. *Biophys. J.* **1993**, *64*, 443−453.

(15) Mui, B. L.-S.; Döbereiner, H.-G.; Madden, T. D.; Cullis, P. R. Influence of Transbilayer Area Asymmetry on the Morphology of Large Unilamellar Vesicles. *Biophys. J.* **1995**, *69*, 930−941.




DOI: 10.1021/acs.nanolett.9b02646
*Nano Lett.* 2019, 19, 7703−7711

(16) Frederik, P. M.; Hubert, D. H. W. *Cryoelectron Microscopy of Liposomes*; Elsevier, 2005; Vol. *391*.
(17) Dragicevic-Curic, N.; Scheglmann, D.; Albrecht, V.; Fahr, A. Temoporfin-Loaded Invasomes: Development, Characterization and In Vitro Skin Penetration Studies. *J. Controlled Release* **2008**, *127*, 59−69.
(18) Danino, D. Cryo-TEM of Soft Molecular Assemblies. *Curr. Opin. Colloid Interface Sci.* **2012**, *17*, 316−329.
(19) Goetz, R.; Lipowsky, R. Computer Simulations of Bilayer Membranes: Self-Assembly and Interfacial Tension. *J. Chem. Phys.* **1998**, *108*, 7397−7409.
(20) Yamamoto, S.; Maruyama, Y.; Hyodo, S.-A. Dissipative Particle Dynamics Study of Spontaneous Vesicle Formation of Amphiphilic Molecules. *J. Chem. Phys.* **2002**, *116*, 5842.
(21) Marrink, S. J.; Mark, A. E. Molecular Dynamics Simulation of the Formation, Structure, and Dynamics of Small Phospholipid Vesicles. *J. Am. Chem. Soc.* **2003**, *125*, 15233−15242.
(22) Seifert, U.; Berndl, K.; Lipowsky, R. Shape Transformations of Vesicles: Phase Diagram for Spontaneous Curvature and Bilayer Coupling Model. *Phys. Rev. A: At., Mol., Opt. Phys.* **1991**, *44*, 1182−1202.
(23) Miao, L.; Seifert, U.; Wortis, M.; Döbereiner, H.-G. Budding Transitions of Fluid−Bilayer Vesicles: the Effect of Area−Difference Elasticity. *Phys. Rev. E: Stat. Phys., Plasmas, Fluids, Relat. Interdiscip. Top.* **1994**, *49*, 5389−5407.
(24) Seifert, U. Configurations of Membranes and Vesicles. *Adv. Phys.* **1997**, *46*, 13−137.
(25) Lipowsky, R. Understanding Giant Vesicles—A Theoretical Perspective. In *The Giant Vesicle Book*; Dimova, R., Marques, C., Eds.; Taylor & Francis, 2019.
(26) Rozycki, B.; Lipowsky, R. Spontaneous Curvature of Bilayer Membranes from Molecular Simulations: Asymmetric Lipid Densities and Asymmetric Adsorption. *J. Chem. Phys.* **2015**, *142*, 054101.
(27) Sreekumari, A.; Lipowsky, R. Lipids with Bulky Head Groups Generate Large Membrane Curvatures by Small Compositional Asymmetries. *J. Chem. Phys.* **2018**, *149*, 084901.
(28) Winterhalter, M.; Helfrich, W. Bending Elasticity of Electrically Charged Bilayers: Coupled Monolayers, Neutral Surfaces, and Balancing Stresses. *J. Phys. Chem.* **1992**, *96*, 327−330.
(29) Templer, R. H. On the Area Neutral Surface of Inverse Bicontinuous Cubic Phases of Lyotropic Liquid Crystals. *Langmuir* **1995**, *11*, 334−340.
(30) Rowlinson, J.; Widom, B. *Molecular Theory of Capillarity*; Clarendon Press: Oxford, 1989.
(31) Nakamura, T.; Kawamoto, S.; Shinoda, W. Precise Calculation of the Local Pressure Tensor in Cartesian and Spherical Coordinates in LAMMPS. *Comput. Phys. Commun.* **2015**, *190*, 120−128.
(32) Satarifard, V.; Grafmüller, A.; Lipowsky, R. Nanodroplets at Membranes Create Tight-Lipped Membrane Necks via Negative Line Tension. *ACS Nano* **2018**, *12*, 12424−12435.
(33) Miettinen, M.; Lipowsky, R. Bilayer Membranes with Frequent Flip Flops have Tensionless Leaflets. *Nano Lett.* **2019**, *19*, 5011.
(34) Fournier, J. B. On the Stress and Torque Tensors in Fluid Membranes. *Soft Matter* **2007**, *3*, 883−888.
(35) Deserno, M. Fluid Lipid Membranes: From Differential Geometry to Curvature Stresses. *Chem. Phys. Lipids* **2015**, *185*, 11−45.
(36) Goetz, R.; Gompper, G.; Lipowsky, R. Mobilitiy and Elasticity of Self-Assembled Membranes. *Phys. Rev. Lett.* **1999**, *82*, 221−224.
(37) Döbereiner, H.-G.; Evans, E.; Kraus, M.; Seifert, U.; Wortis, M. Mapping Vesicle Shapes into the Phase Diagram: A Comparison of Experiment and Theory. *Phys. Rev. E: Stat. Phys., Plasmas, Fluids, Relat. Interdiscip. Top.* **1997**, *55*, 4458−4474.
(38) Möbius, W.; van Donselaar, E.; Ohno-Iwashita, Y.; Shimada, Y.; Heijnen, H. F. G.; Slot, J. W.; Geuze, H. J. Recycling Compartments and the Internal Vesicles of Multivesicular Bodies Harbor Most of the Cholesterol Found in the Endocytic Pathway. *Traffic* **2003**, *4*, 222−231.
(39) Skotland, T.; Hessvik, N. P.; Sandvig, K.; Llorente, A. Exosomal Lipid Compostion and the Role of Ether Lipids and Phosphinositides in Exosome Biology. *J. Lipid Res.* **2019**, *60*, 9−18.
(40) Zabeo, D.; Cvjetkovic, A.; Lässer, C.; Schorb, M.; Lötvall, J.; Höög, J. L. Exosomes Purified from a Single Cell Type have Diverse Morphology. *J. Extracell. Vesicles* **2017**, *6*, 1329476.
(41) Oliveira, D. L.; Rizzo, J.; Joffe, L. S.; Godinho, R. M. C.; Rodrigues, M. L. Where Do They Come from and Where Do They Go: Candidates for Regulating Extracellular Vesicle Formation in Fungi. *Int. J. Mol. Sci.* **2013**, *14*, 9581−9603.
(42) Beer, K. B.; Rivas-Castillo, J.; Kuhn, K.; Fazeli, G.; Karmann, B.; Nance, J. F.; Stigloher, C.; Wehman, A. M. Extracellular Vesicle Budding is Inhibited by Redundant Regulators of TAT-5 Flippase Localization and Phospholipid Asymmetry. *Proc. Natl. Acad. Sci. U. S. A.* **2018**, *115*, E1127−E1136.
(43) Plimpton, S. Fast Parallel Algorithms for Short-Range Molecular Dynamics. *J. Comput. Phys.* **1995**, *117*, 1−19.
(44) Martínez, L.; Andrade, R.; Birgin, E. G.; Martínez, J. M. PACKMOL: a Package for Building Initial Configurations for Molecular Dynamics simulations. *J. Comput. Chem.* **2009**, *30*, 2157−2164.



DOI: 10.1021/acs.nanolett.9b02646
*Nano Lett.* 2019, 19, 7703−7711